Atmospheric and
Environmental Research, Inc.

Two-Dimensional Transport Studies for the Composition and Structure of the Io Plasma Torus

ATMOSPHERIC AND ENVIRONMENTAL RESEARCH, INC.
LEXINGTON, MASSACHUSETTS

December 29, 2003

Two-Dimensional Transport Studies for the Composition and Structure of the Io Plasma Torus

William H. Smyth

Atmospheric and Environmental Research, Inc.
131 Hartwell Avenue
Lexington, MA 02421-3126

Report for the Period of
December 19, 2002 to December 18, 2003

I. Introduction

The overall objective of this project is to investigate the roles of local and spatially extended plasma sources created by Io, plasma torus chemistry, and plasma convective and diffusive transport in producing the long-lived S^+, S^{++} and O^+ radial "ribbon" structures of the plasma torus, their System III longitude and local-time asymmetries, their energy sources and their possible time variability. To accomplish this objective, two-dimensional [radial (L) and System III longitude] plasma transport equations for the flux-tube plasma content and energy content will be solved that include the convective motions for both the east-west electric field and corotational velocity-lag profile near Io's orbit, radial diffusion, and the spacetime dependent flux-tube production and loss created by both neutral-plasma and plasma-ion reaction chemistry in the plasma torus. For neutral-plasma chemistry, the project will for the first time undertake the calculation of realistic three-dimensional, spatially-extended, and time-varying contributions to the flux-tube ion-production and loss that are produced by Io's corona and extended neutral clouds. The unknown two-dimensional spatial nature of diffusion in the plasma transport will be isolated and better defined in the investigation by the collective consideration of the foregoing different physical processes. For energy transport, the energy flow from hot pickup ions (and a new electron source) to thermal ions and electrons will be included in investigating the System III longitude and local-time temperature asymmetries in the plasma torus. The research is central to the scope of the NASA Sun-Earth Connection Roadmap in Quest II Campaign 4 "Comparative Planetary Space Environments" by addressing key questions for understanding the magnetosphere of planets with high rotation rates and large internal plasma sources and, in addition, is of considerable importance to the NASA Solar System Exploration Science Theme. In this regard, Jupiter is the most extreme example with its rapid rotation and with its inner Galilean satellite Io providing the dominant plasma source for the magnetosphere. The research work is furthermore highly relevant to the scientific goals and the ongoing interpretation of data for the Jupiter system acquired by a host of ground-based facilities, the Hubble Space Telescope,

Table 1. Three-Year Research Plan

Investigation	Year 1	Year 2	Year 3
Step 1: Calculations for Iogenic plasma sources & lifetimes	Calculate Outer Source ion/energy productions, ion loss lifetimes, and explore Inner Sources.	Complete Outer Source calculations; continue to explore impact of molecular sources and sinks for the plasma torus chemistry.	
Step 2: Transport studies for $N_i L^2$	Add corotational-lag convection to transport equations; perform exploratory calculations.	Undertake major transport calculations for the spatial structure of the torus for an Inner Source and also Outer Source atomic sources and important molecular contributions; publish results.	
Step 3: Transport studies for ε_i and $N_i L^2$	--	Initiate energy transport studies; explore power of Outer Source and Inner Source and torus System III longitude and local-time asymmetries.	

the Voyager, Ulysses, and Galileo missions, and by the Cassini mission in its recent Jupiter flyby. The three-year research plan is summarized in Table 1.

II. Summary of Work Performed in the First Project Year

In the first project year, research efforts have been focused upon a refinement and assessment of the neutral-plasma processes and the plasma-plasma processes in the plasma torus and the initiation of calculations for the associated production and loss rates for the primary heavy ion species S^+, S^{++}, S^{+++}, O^+, and O^{++}. In addition, research efforts have been directed to developing a formalism for the plasma convection velocities introduced by the east-west electric field and by corotational lag near Io's orbit and thereby to develop an appropriate description for the subcorotational velocity of the plasma torus as a function of System III longitude and radial L-shell. The plasma transport equations and the major activities undertaken in the first project year to develop a description of the sources, sinks, and convective velocities required in these equations are summarized below.

2.1 Plasma Transport Equations

The two-dimensional transport equations for a flux tube located at the magnetic radial L shell and a System III longitude ϕ with cross sectional area $LdLd\phi$ are given for the flux tube ion-content conserved quantity $N_i L^2$ of the i-species as follows:

$$\frac{\partial(N_i L^2)}{\partial t} + (V_{E-W}^{(L)} + V_{Lag}^{(L)})\frac{\partial(N_i L^2)}{\partial L} + \frac{V_{Lag}^{(\phi)}}{L}\frac{\partial(N_i L^2)}{\partial \phi} - L^2 \frac{\partial}{\partial L}\left(\frac{D_{LL}}{L^2}\frac{\partial(N_i L^2)}{\partial L}\right) = P_i^{(N)}(L,\phi,t) - L_i^{(N)}(L,\phi,t). \quad (1)$$

The quantities $N_i(L,\phi,t)$, $P_i^{(N)}(L,\phi,t)$, and $L_i^{(N)}(L,\phi,t)$ are, respectively, the number of ions, the instantaneous ion production rate, and the instantaneous ion loss rate for the flux tube per unit $dLd\phi$. On the left-hand side of Eq. 1, the quantity $V_{E-W}^{(L)}$ is the L component of the periodic convection velocity produced by the east-west electric field, which moves the plasma initially on an L shell at Io's orbit radially outward by ~0.3 R_J as the plasma corotates from the west (dusk) to the east (dawn) ansa. For plasma created at the eastern (dawn) and western (dusk) ansa, their trajectories about Jupiter are illustrated in Figure 1. The small change in radial location of the plasma trajectories is important because it preferentially exposes the plasma that is initially created by Io when west of Jupiter (and subsequently moves east of Jupiter) to a larger L and a smaller magnetic field and hence to more rapid outward radial diffusion than for plasma that is initially created by Io when east of Jupiter (Smyth and Marconi 1998). The ϕ component, $V_{E-W}^{(\phi)}$, of the east-west convective motion of the plasma as it moves about Jupiter is small and periodic (~± 1.5°) and is neglected in Eq. 1. The convection velocity $V_{E-W}^{(L)}$ depends upon L and also its

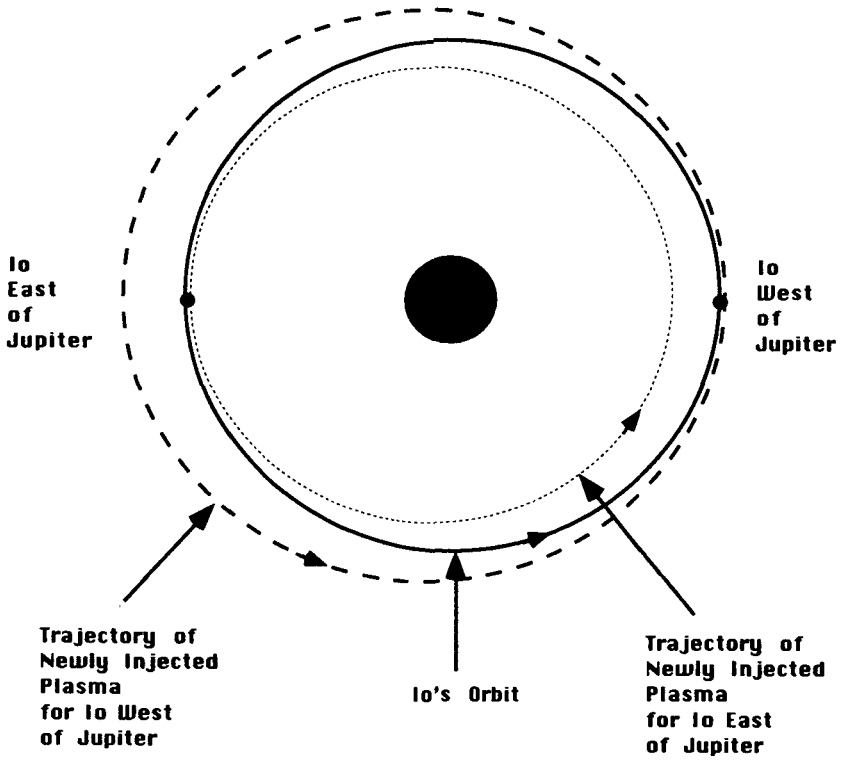

Figure 1. Motion about Jupiter of Plasma Created by an Io Source. The trajectories in the plasma torus of newly injected plasma from Io (represented by the dot on the satellite's solid-line circular orbit) are shown for Io east of Jupiter by the dotted blue circle and for Io west of Jupiter by the dashed-line red circle. Jupiter is shown to scale by the central filled circle. The figure was taken from Smyth and Marconi (1998).

local-time angle about Jupiter. The quantity $V_{Lag}^{(L)}$ and $V_{Lag}^{(\phi)}$ are the L and ϕ components of the convection velocity produced by the corotational-lag velocity-trough centered near or at Io's orbit. The convective plasma corotational-lag acts to homogenize flux-tube enhancements in ϕ that would otherwise exist because of the larger plasma sources created in the higher plasma densities near ϕ=112-130° and 292° as Io moves both radially and latitudinally within and/or across the plasma torus centrifugal-equator plane. The presence of this corotational lag is also thought to be essential to stabilize the observed long-lived torus structures from resonance effects between the inward-outward motions of the plasma caused by the east-west field and the modulation of this motion by the System III rotation period of Jupiter's magnetic field (Zhan and Hill 2000). The quantity D_{LL} is the radial diffusion coefficient, which has a strong dependence on L and is also considered here to be, in general, a function of ϕ and its local-time angle about Jupiter. On the right-hand side of Eq. 1, the production rates $P_i^{(N)}(L,\phi,t)$ and loss rates $L_i^{(N)}(L,\phi,t)$ for the i-species include a significant number of chemical reactions for plasma-neutral and plasma-plasma processes.

2.2 Chemistry in the Io Plasma Torus

An updated list of the chemical reactions for the production and loss of ion species in the plasma torus is summarized in Table 2. The set of 49 reactions is divided into six different categories, which collectively contains 33 neutral-plasma reactions and 16 plasma-plasma reactions. Electron impact processes contribute to 22 of the reactions: 7 atomic ionization reactions, 9 molecular ionization/dissociation reactions, and 6 recombination reactions. Ion processes contribute to the remaining 27 reactions: 14 atom-ion charge exchange reactions, 10 molecule-ion charge exchange reactions, and 3 ion-ion charge exchange reactions. In our previous exploratory two-dimensional [radial (L) and System III longitude] plasma transport calculations for S^+ and S^{++}, torus chemistry was limited to only the six red reactions for S to specify the primary production rate of S^+ and the one green reaction for S^+ to specify the primary loss rate of S^+ and the primary production rate of S^{++}. The situation for the plasma transport of S^+ and S^{++} is clearly much more complex than this earlier treatment since both additional production and loss contributions are also provided by the reactions involving O, SO, and SO_2. This same situation also exists for plasma transport calculations of O^+ and O^{++}, which are also to be undertaken in this project.

Table 2. Chemistry In the Io Plasma Torus

Atomic Ionization Reactions

k1 $e + S \rightarrow S^+ + 2e$
k2 $e + S^+ \rightarrow S^{++} + 2e$
k3 $e + S^{++} \rightarrow S^{+++} + 2e$
k4 $e + S^{+++} \rightarrow S^{++++} + 2e$
k5 $e + O \rightarrow O^+ + 2e$
k6 $e + O^+ \rightarrow O^{++} + 2e$
k7 $e + O^{++} \rightarrow O^{+++} + 2e$

Atom-Ion Reactions

k8 $S + S^+ \rightarrow S^+ + S$
k9 $S + S^{++} \rightarrow S^{++} + S$
k10 $S + S^{++} \rightarrow S^+ + S^+$
k11 $S + S^{+++} \rightarrow S^+ + S^{++}$
k12 $S + S^{+++} \rightarrow S^{++} + S^+$
k13 $S + O^+ \rightarrow S^+ + O$
k14 $S + O^{++} \rightarrow S^+ + O^+$
k15 $S + O^{++} \rightarrow S^{++} + O^+ + e$
k16 $O + O^+ \rightarrow O^+ + O$
k17 $O + O^{++} \rightarrow O^{++} + O$
k18 $O + O^{++} \rightarrow O^+ + O^+$
k19 $O + S^+ \rightarrow O^+ + S$
k20 $O + S^{++} \rightarrow O^+ + S^+$
k21 $O + S^{+++} \rightarrow O^+ + S^{++}$

Ion-Ion Reactions

k22 $S^+ + O^{++} \rightarrow S^{++} + O^+$
k23 $S^+ + S^{+++} \rightarrow S^{++} + S^{++}$
k24 $S^{++} + O^{++} \rightarrow S^{+++} + O^+$

Molecule-Ion Reactions

k25 $SO + S^+ \rightarrow SO^+ + S$
k26 $SO + S^{++} \rightarrow SO^+ + S^+$
k27 $SO + S^{+++} \rightarrow SO^+ + S^{++}$
k28 $SO + O^+ \rightarrow SO^+ + O$
k29 $SO + O^{++} \rightarrow SO^+ + O^+$
k30 $SO_2 + S^+ \rightarrow SO_2^+ + S$
k31 $SO_2 + S^{++} \rightarrow SO_2^+ + S^+$
k32 $SO_2 + S^{+++} \rightarrow SO_2^+ + S^{++}$
k33 $SO_2 + O^+ \rightarrow SO_2^+ + O$
k34 $SO_2 + O^{++} \rightarrow SO_2^+ + O^+$

Recombination Reactions

k35 $e + S^+ \rightarrow S$
k36 $e + S^{++} \rightarrow S^+$
k37 $e + S^{+++} \rightarrow S^{++}$
k38 $e + SO^+ \rightarrow S + O$
k39 $e + SO_2^+ \rightarrow SO + O$
k40 $e + SO_2^+ \rightarrow S + O_2$

Electron-Molecular Reactions

k41 $e + SO \rightarrow SO^+ + 2e$
k42 $e + SO \rightarrow S^+ + O + 2e$
k43 $e + SO \rightarrow S + O^+ + 2e$
k44 $e + SO^+ \rightarrow S^+ + O + e$
k45 $e + SO_2 \rightarrow SO_2^+ + 2e$
k46 $e + SO_2 \rightarrow SO^+ + O + 2e$
k47 $e + SO_2 \rightarrow S^+ + O_2 + 2e$
k48 $e + SO_2 \rightarrow SO + O^+ + 2e$
k49 $e + SO_2^+ \rightarrow SO^+ + O + e$

2.3 Production and Loss Rates in the Plasma Torus

The instantaneous ion production rates, $P_i^{(N)}(L,\phi,t)$, and the instantaneous ion loss rates, $L_i^{(N)}(L,\phi,t)$, for the flux tube content per unit $dLd\phi$ are required to solve Eq. 1 for the time evolution of the two-dimensional plasma transport. These production and loss rates can be divided, as introduced by Smyth and Marconi (2003a,b), into an Inner Region source, originating

below Io's exobase, and an Outer Region source, originating above Io's exobase in the gravitationally bound satellite corona and its escaping neutral clouds. The Inner Region source is essentially a point source at Io's instantaneous location for which the production source rate in the transport model may be specified. For the Outer Region source, the relevant ion production and loss contributions for neutral-plasma reactions are specified by the calculated volumetric ion production and loss rates as determined by the neutral cloud models for O, S, SO and SO_2 for suitably defined exobase source conditions and for the subsequent plasma torus chemistry in Table 2.

Efforts in the first project year have been directed to the assessment and to the calculation of the associated instantaneous ion production and loss rates that are created for the Outer Source by Io's neutral clouds for O, S, SO, and SO_2 and their interactions in the plasma torus summarized in Table 2. The primary focus of this effort has been for the sulfur ion family of species S^+, S^{++}, and S^{+++} which create a sequence of observed radial peaks (or so-called "ribbon" features) in the plasma for S^+ (at ~5.3 and 5.6 R_J) and S^{++} (at 5.6 R_J), as illustrated by in Figure 2.

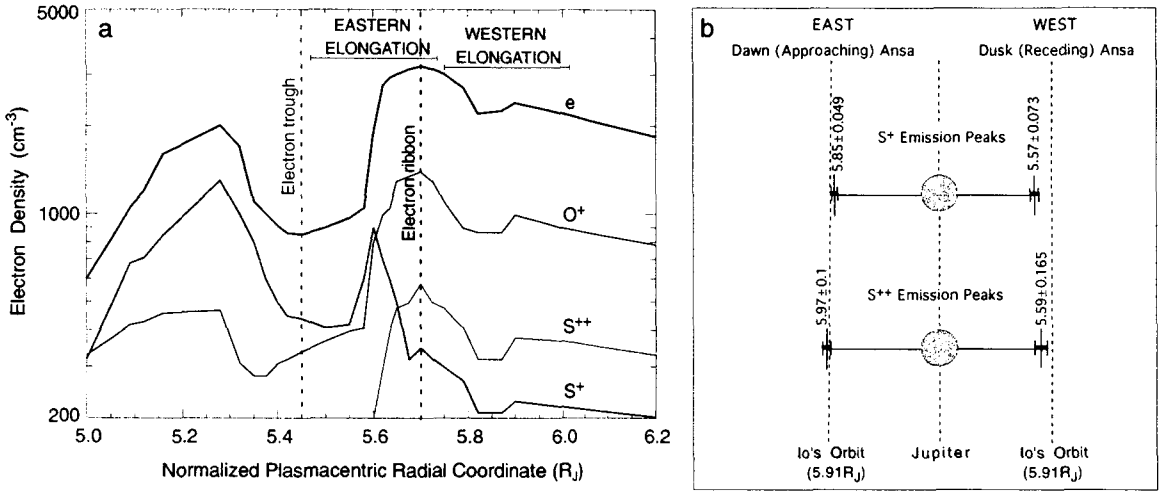

Figure 2. Ribbon Structure in the Plasma Torus. In (a), the Voyager-epoch density profiles (Bagenal 1994) for electrons (e), O^+, S^+, and S^{++} in the plasma torus centrifugal plane are shown in the normalized $[\tilde{L}/(1+\varepsilon)]$ plasmacentric radial coordinate (Smyth and Combi 1988a), where the ion and electron densities are fixed in location, but Io's motion at eastern and western elongations is indicated. In (b), the east-west asymmetry of the average radial location (exaggerated scale for clarity) and the System III longitude variation about this average location (dark bars) for the observed peak intensity of S^+ (6731 Å) and S^{++} (685 Å) emissions are illustrated relative to Io's orbit and Jupiter (Smyth and Marconi 1998a). In (a), the radial locations of the electron ribbon and electron trough are indicated by dashed lines.

The sulfur ions S^+ and S^{++} are generally more abundant than S^{+++} (not shown in Figure 2) because of their smaller ionization potentials of 10.36 eV for S and 23.33 eV for S^+ as compared to the larger ionization potential of 34.83 eV for S^{++}. Near Io's orbit, the thermal electron temperature

of ~5 eV is small compared to all of these ionization potentials, but the electron temperature increases radially outward. The oxygen ion family consists primarily of O^+, which has a radial peak at ~5.7 R_J, and a small concentration (typically ~few percent) of O^{++} (not shown in Figure 2), which also has a radial peak near ~5.7 R_J. Near Io's orbit, the small concentration of O^{++} is attributed to the large ionization potential of 35.12 eV for O^+, which is comparable to the ionization potential for S^{++} for the creation of S^{+++}.

For the sulfur ion family of species S^+, S^{++}, and S^{+++}, the System III longitude-averaged radial profiles in the plasma torus equator plane are illustrated for the electron impact ionization rate (reciprocal of the lifetime) in Figure 3 and for the electron impact recombination rate (reciprocal of the lifetime) in Figure 4, as created by the thermal electron population of the plasma torus. As expected, the ionization rates for thermal electrons are larger for the ion species with the lower ionization potentials. In addition to thermal electrons, the plasma torus also contains a nonthermal electron population that appears to be time-dependent and is not particularly well understood. Voyager spacecraft measurements (Bagenal 1994) suggest that nonthermal electrons near Io's orbit may be characterized by a temperature of ~100 eV and a

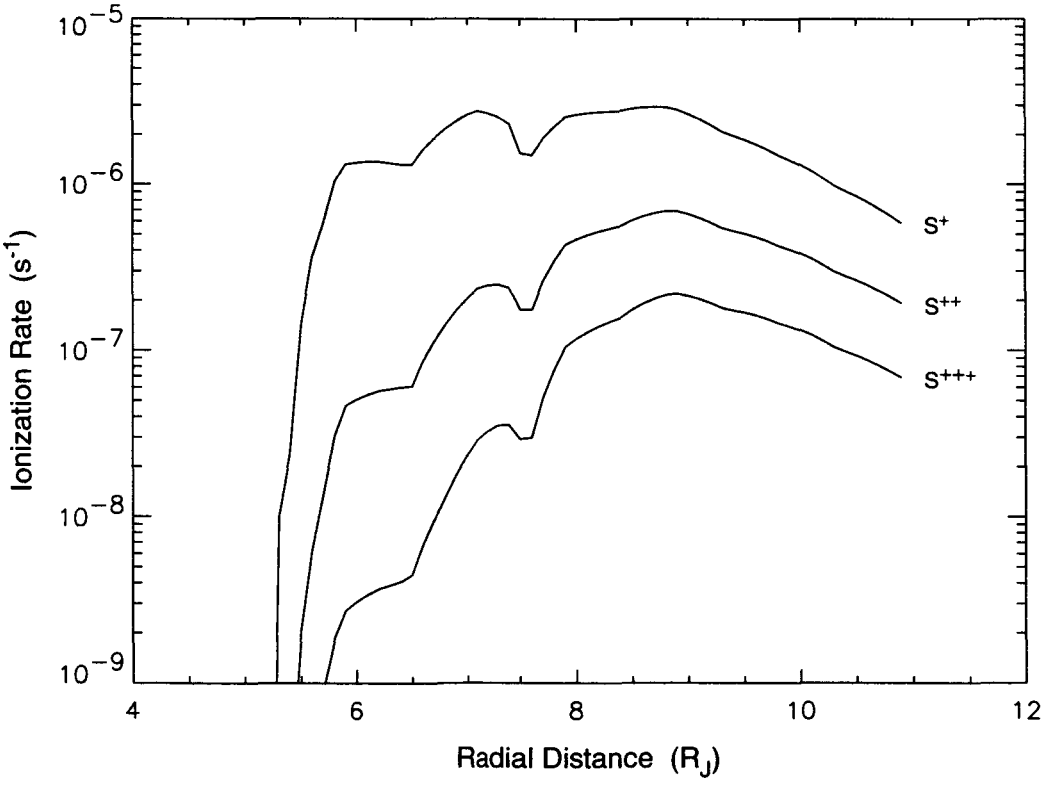

Figure 3. Radial Profiles for the Ionization Rate of S^+, S^{++}, S^{+++}. The System III longitudinally-averaged radial profiles for the ionization rates of S^+, S^{++}, and S^{+++} in the centrifugal equatorial plane of the plasma torus created by the thermal electron population are shown for Voyager 1 epoch plasma conditions.

nonthermal to thermal density ratio of $\leq 10^{-3}$. In addition, similar erratic time variations in the observed [O I] 6300 Å emissions from Io (Oliversen et al. 2001) and in Galileo spacecraft PLS measurements for electrons (Paterson 2000) indicate an erratic non-thermal electron component in the plasma torus that is characterized by a temperature of ~30 eV and a non-thermal to thermal density ratio of $\sim 10^{2}$. Based upon the temperature-dependent profile for the ionization reaction rates per electron presented in Figure 5, it can be seen that the ~30 eV and ~100 eV non-thermal electron populations have somewhat similar rates, which are much larger than the rates for the ~5eV thermal electrons and which become relatively larger with increasing ionization potential of the species. Because of this behavior, the non-thermal electrons have only a small impact on the ionization rate of S to create S^{+}, a moderate impact on the ionization rate of S^{+} to create S^{++}, and a dominant impact on the ionization rate of S^{++} to create S^{+++} and S^{+++} to create S^{++++}. Hence the non-thermal electron populations will play an important role in populations of the sulfur ion family of species S^{+}, S^{++}, and S^{+++} and is currently being included in the production and loss rates of Eq. 1. For S^{+}, the recombination rate in Figure 4 is much smaller than the ionization rates in Figure 3 everywhere except within Io's orbit, where the electron temperature rapidly decreases with decreasing radial distance. For the higher charged states, however, the recombination rate

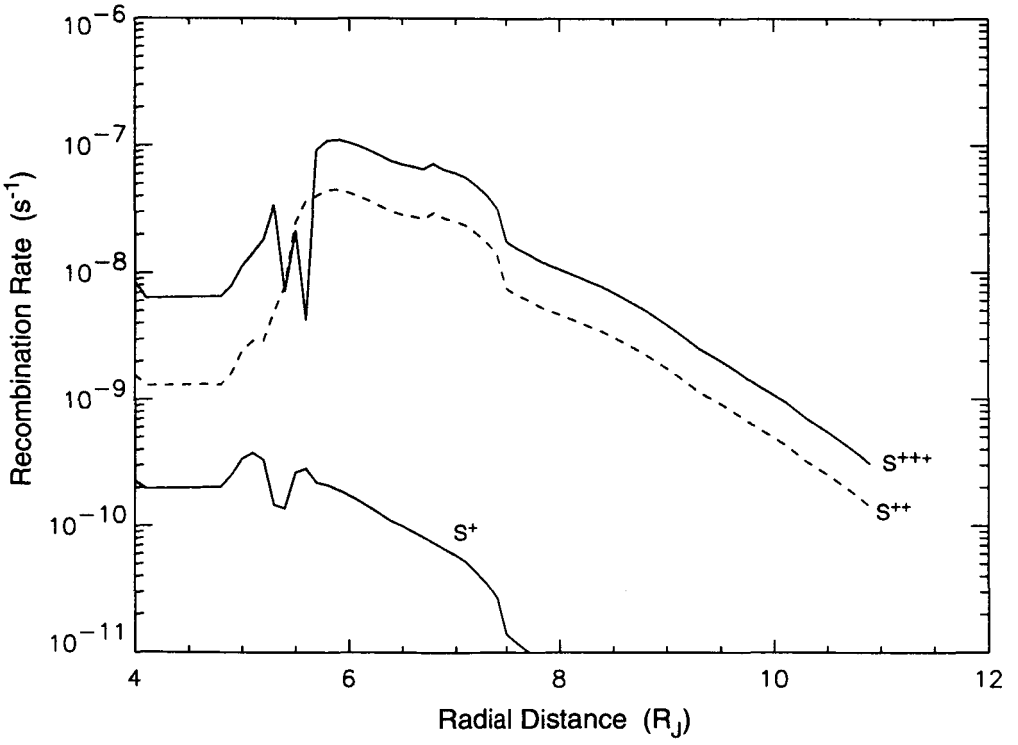

Figure 4. Radial Profiles for the Recombination Rate of S^{+}, S^{++}. S^{+++}. The System III longitudinally-averaged radial profiles for the electron recombination rates of S^{+}, S^{++}, and S^{+++} in the centrifugal equatorial plane of the plasma torus created by the thermal electron population are shown for Voyager 1 epoch plasma conditions.

for S^{++} is more competitive with the ionization rates over a wider radial range near Io's orbit and for S^{+++} over a radial range well beyond Io's orbit.

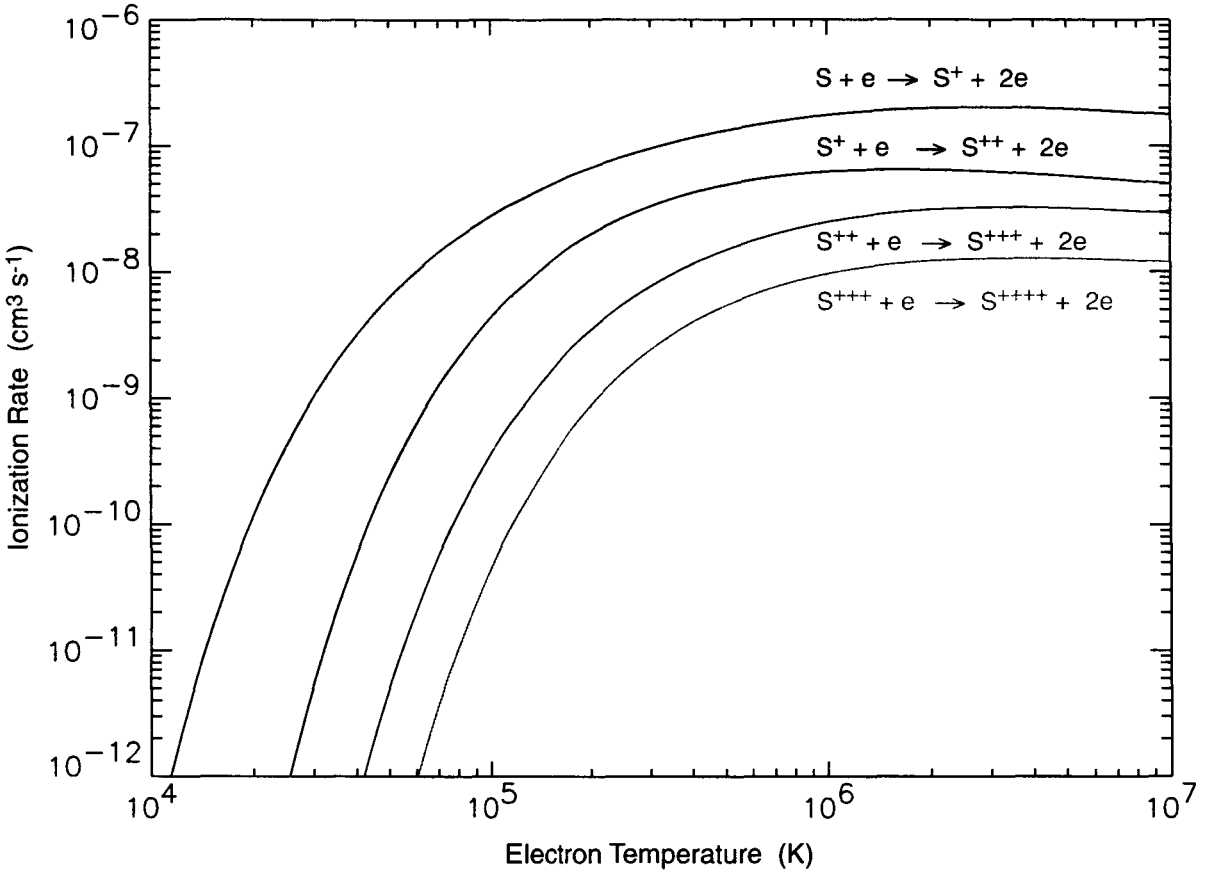

Figure 5. Electron Impact Reaction Rate for Ionization of S, S^+, S^{++}, and S^{+++}. The dependence of the electron impact reaction rates for ionization of S, S^+, S^{++}, and S^{+++} are shown as a function of electron temperature.

In addition to electron impact ionization and recombination reactions, ion-neutral and ion-ion reactions in Table 2 also contribute to the ion production and loss terms for the Outer Source region. For the Outer Source only, the circumplanetary two-dimensional distribution for the time-averaged net-production rate, $\langle P_i^{(N)}(L,\phi,t) - L_i^{(N)}(L,\phi,t)\rangle$, integrated along the magnetic field lines and calculated for the reactions k1, k2, k3, k4, k10, k11, k12, k13, k14, k18, k19, k35, k36, and k37 of Table 2 is presented for S^+, S^{++}, and S^{+++}, respectively, in Figures 6, 7, and 8. These net ion production rates are calculated for the plasma properties for the Voyager-epoch plasma torus description adopted in the neutral cloud model. In Figure 6, the net S^+ production rate is positive and highly peaked about Io's orbit. In Figure 7, the net S^{++} production rate is positive and highly peaked at Io's orbit but becomes negative in a narrow radial interval just inside of Io's orbit. In Figure 8, the net S^{+++} production rate is negative everywhere with its largest negative values outside on Io's orbit. Corresponding ion rates for the Outer Region

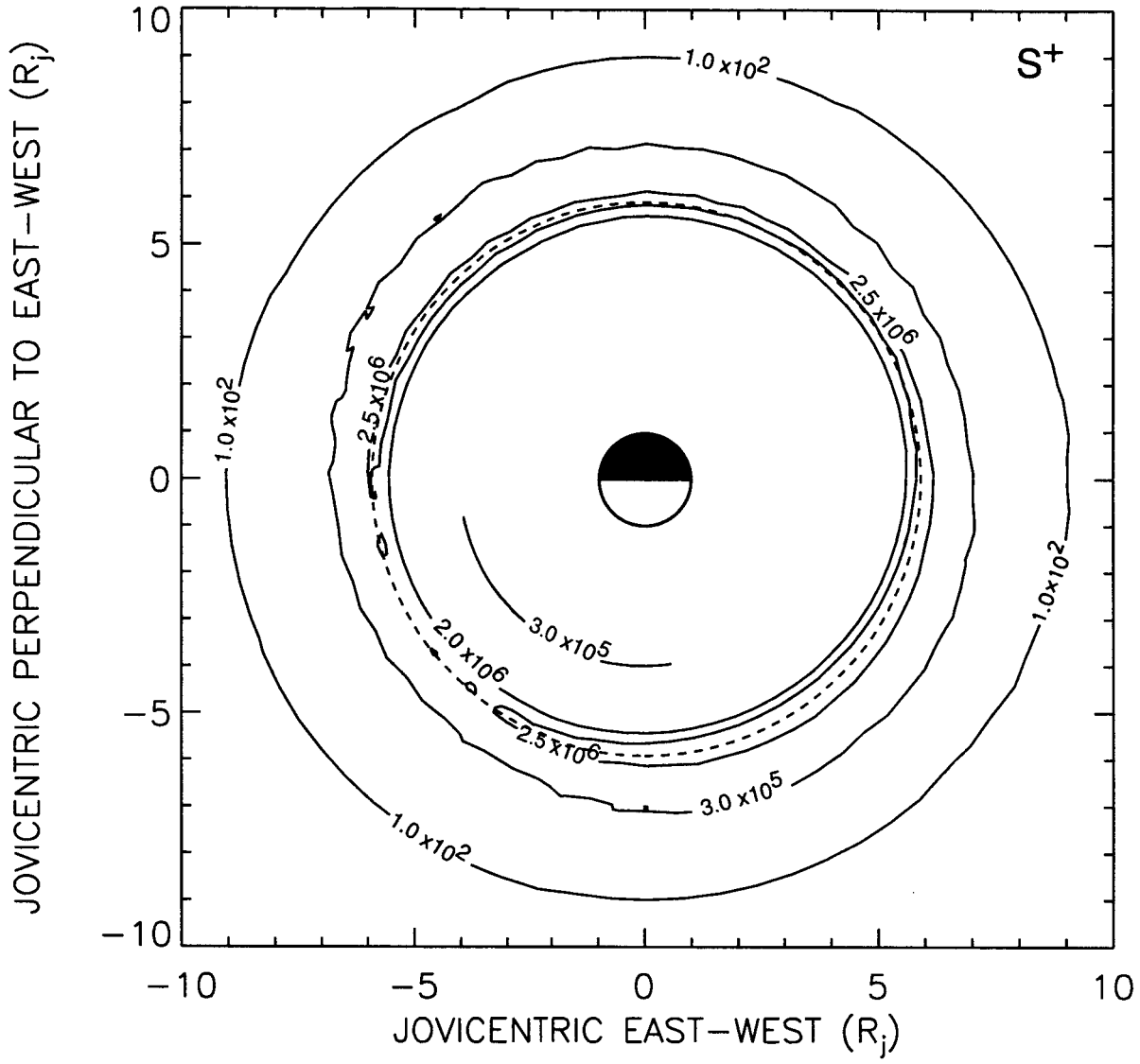

Figure 6. Time-Averaged Net Production Rate of S^+ from Neutrals. The circumplanetary two-dimensional distribution for the S^+ net production rate (ions cm^{-2} s^{-1}) integrated along the magnetic field and time-averaged over 484 samples separated by 2100 s and created by Io's neutral O and S neutral clouds is shown. The source rates for the O and S clouds are 1.38 $x10^{28}$ and 0.69 $x10^{28}$ atoms s^{-1} ejected isotropically from Io's exobase with a simple monoenergetic speed of 2.6 km s^{-1}.

source have also been calculated for the SO_2 and SO neutral clouds. More complete rates will be calculated early in the second project year. Very preliminary and exploratory transport calculations have also been undertaken for S^+, S^{++}, and S^{+++} near the end of the first project year that include both an adopted Inner Region source as well as various contributions for the Outer Region source. The S^+ ribbon, determined primarily by the ions created by the Inner Region, and

the S^{++} ribbon, determined primarily by electron impact ionization of outward transported S^{+}, have about the correct radial locations and but not yet the correct N_iL^2 values when compared to Voyager-epoch results (Bagenal 1994). A proper comparison of the N_iL^2 values at larger radial distances for S^{+}, S^{++}, and S^{+++} as well as for O^{+} and O^{++} will require the inclusion of a velocity distribution for the Outer Region source to be undertaken early in the second project year.

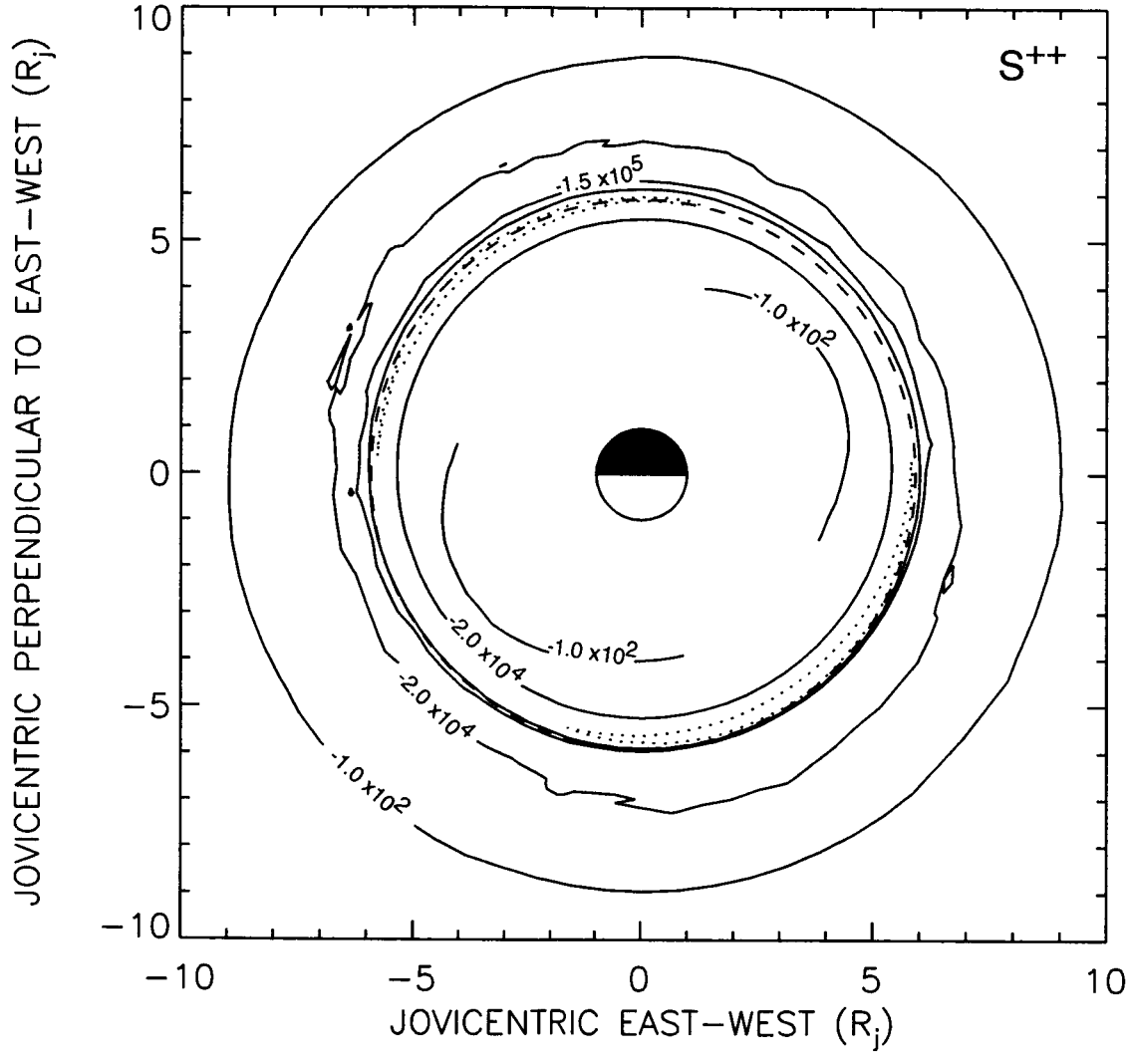

Figure 7. Time-Averaged Net Production Rate of S^{++} from Neutrals. The circumplanetary two-dimensional distribution for the S^{++} net production rate (ions cm^{-2} s^{-1}) integrated along the magnetic field and time-averaged over 484 samples separated by 2100 s and created by Io's neutral O and S neutral clouds is shown. The source rates for the O and S clouds are 1.38 $x10^{28}$ and 0.69 $x10^{28}$ atoms s^{-1} ejected isotropically from Io's exobase with a simple monoenergetic speed of 2.6 km s^{-1}. The dotted contour is negative with a value of -3.5 x 10^5 ions cm^{-2} s^{-1}.

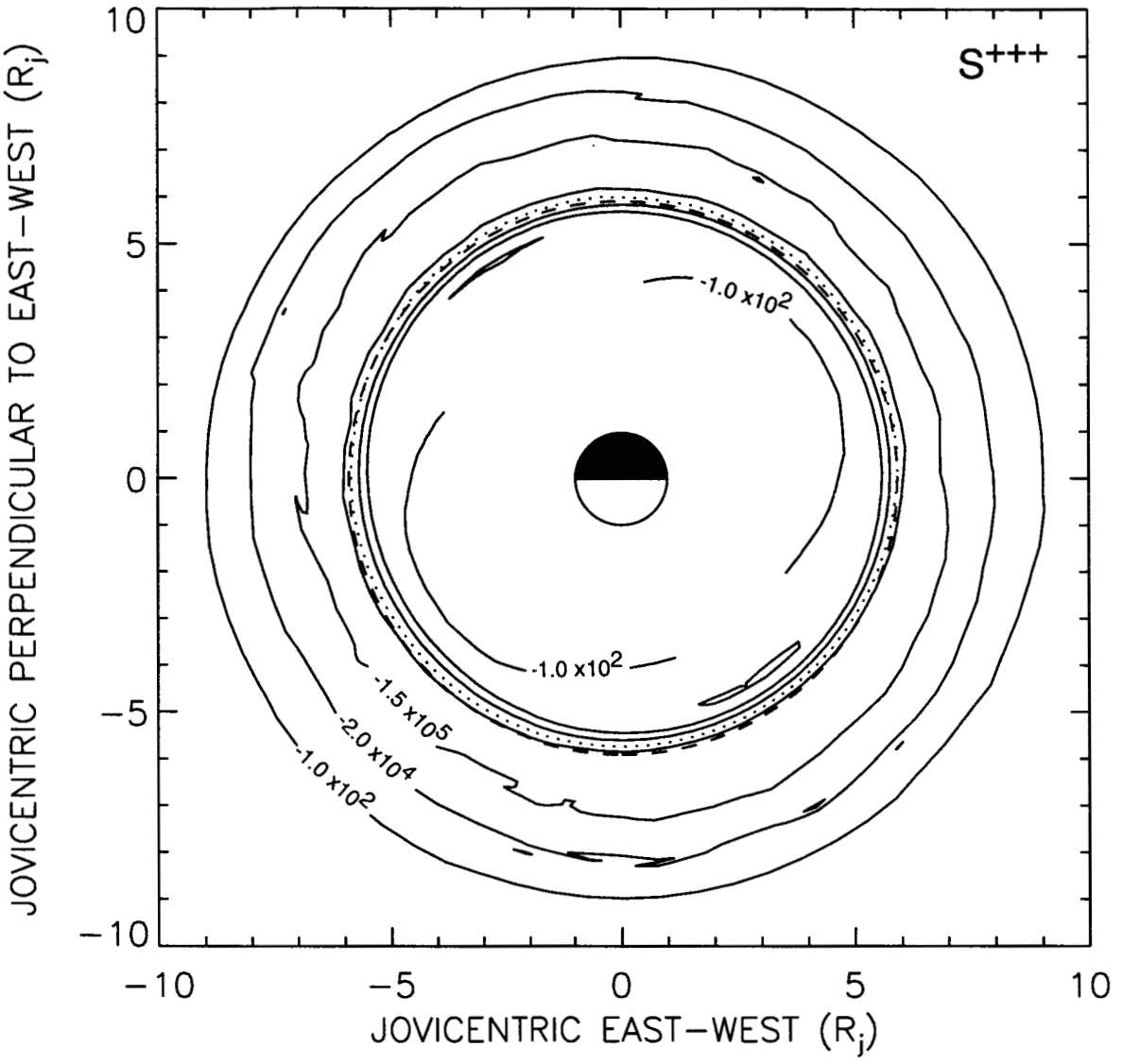

Figure 8. Time-Averaged Net Production Rate of S^{+++} from Neutrals. The circumplanetary two-dimensional distribution for the S^{+++} net production rate (ions cm^{-2} s^{-1}) integrated along the magnetic field and time-averaged over 484 samples separated by 2100 s and created by Io's neutral O and S neutral clouds is shown. The source rates for the O and S clouds are 1.38 $x10^{28}$ and 0.69 $x10^{28}$ atoms s^{-1} ejected isotropically from Io's exobase with a simple monoenergetic speed of 2.6 km s^{-1}. The dotted contour has a value of -2.0 x 10^4 ions cm^{-2} s^{-1} and the inner three solid contours have a value of -100 ions cm^{-2} s^{-1}.

2.4 Corotation of the Io Plasma Torus

A prerequisite to the development of a description for the subcorotational velocities $V_{Lag}^{(L)}$ and $V_{Lag}^{(\phi)}$ of the plasma torus in Eq. 1 is to understand how the corotation convection velocity is

established in the plasma torus. A framework for the corotation of the plasma torus may be formulated in terms of a description for the electric and magnetic fields. For the more complex magnetic field configurations required for the Io plasma torus in Jupiter's inner magnetosphere, the mathematical expressions for the electric and magnetic fields are currently being derived in this project. The basic framework for this development is briefly outlined below.

The velocity $\bar{v}$ of a particle of mass m and charge q in the Io plasma torus in the presence of an electromagnetic force $\bar{F}$ and in the absence of collisions with neutral species is determined in an inertial frame by the solution of the force equation

$$\bar{F} = m\frac{d\bar{v}}{dt} = q(\bar{E} + \bar{v} \times \bar{B}). \tag{2}$$

The electric field $\bar{E}$ and magnetic field $\bar{B}$ are determined by the general solution of Maxwell's equations for the electric potential Φ and vector potential $\bar{A}$ for the magnetic field

$$\bar{E} = -\bar{\nabla}\Phi - \frac{1}{c}\frac{\partial \bar{A}}{\partial t} \tag{3a}$$

$$\bar{B} = \bar{\nabla} \times \bar{A} \tag{3b}$$

for suitably defined conditions for the magnetospheric plasma and for the time dependent nature and boundary conditions of the electrodynamic fields at the planetary surface. For corotation of the inner region of a planetary magnetosphere, it is necessary but not sufficient that the magnetic field morphology be suitably closed in nature and that the magnetospheric plasma along the magnetic field be sufficient in abundance to produce a high electrical conductivity and a suitable polarization charge so that the parallel electric field is zero ($\bar{E}_{||} = 0$) and, hence, so that the condition

$$\bar{E} \cdot \bar{B} = 0 \tag{4}$$

is imposed in the inner magnetosphere.

The solution of Eq. 3 for the electric field $\bar{E}$ and magnetic field $\bar{B}$ for a steady rotating uniformly magnetized and perfectly conducting sphere with arbitrarily aligned axes of rotation and magnetization surrounded by and in contact with a tenuous magnetospheric plasma with infinite conductivity parallel to $\bar{B}$ and zero conductivity perpendicular to $\bar{B}$ was presented by Hones and Bergeson (1965). In that paper, the solution of the vector potential $\bar{A}$ was approximated to be that for a planetary centered and arbitrarily tilted dipole magnetic field, which is appropriate since the current and field produced from the charge polarization are estimated to be small. Given this assumption, the solution for $\bar{E}$ in an inertial frame is then

determined from the condition given by Eq. 4 and depends solely upon the rotation rate and the description of the tilted, rotating dipole magnetic field for $\vec{B}$ and can be written as

$$\vec{E} = -\frac{1}{c}\left[(\vec{\Omega}\times\vec{r})\times\vec{B}\right] \tag{5}$$

where $\vec{\Omega}$ is the angular velocity of the sphere and $\vec{r}$ is the radius vector in spherical coordinates. This solution for $\vec{E}$ is a quadrupole electric field and represents only the component of the induction electric field (created by the second term in Eq. 3a for a tilted, rotating dipole magnetic field) that is perpendicular to $\vec{B}$ where the component of the induction electric field parallel to $\vec{B}$ has been canceled by the electrostatic field for the polarization charge produced by the first term in Eq. 3a. In the non-inertia rotating frame, the electric field is zero, the plasma undergoes no $\vec{E}\times\vec{B}$ drift or energization, and the plasma moves just as it would in a static dipole magnetic field. In the inertial frame for an aligned or anti-aligned dipole magnetic field (i.e., no tilt), the $\vec{E}\times\vec{B}$ drift motion $(\vec{\Omega}\times\vec{r})_{\perp}$ alone causes this corotation. For a non-zero tilt angle for the dipole magnetic field, the $\vec{E}\times\vec{B}$ drift motion $(\vec{\Omega}\times\vec{r})_{\perp}$ alone does not cause this corotation but the combination of all drift motions and the changing gyration energy of the plasma in the induction electric field collectively enforce corotation. A similar solution for more complex magnetic field descriptions such as spinning planetary-centered quadrupole or octupole magnetic fields or an off-set and arbitrarily tilted dipole magnetic field spinning about an axis through the planet's center would therefore also exist for the condition given by Eq. 4 and have an electric field given by Eq. 5.

For the special case of an ideal plasma (Spitzer 1952), the general solution of Eq. 2 for the particle velocity $\vec{v}$ can be approximately represented by the gyration motion of the particle about a point called the "guiding center"

$$\vec{v} = \vec{\omega}_D + \vec{\omega}_{\perp} + \vec{\omega}_{||} \; . \tag{6}$$

The motion of the guiding center perpendicular to $\vec{B}$ is described by the total drift velocity $\vec{\omega}_D$ for the particle, which may be divided into several different physical components, each component of which is the average drift motion that occurs over one complete gyration period. The remaining gyration motion of the particle along $\vec{B}$ is described by its perpendicular $\vec{\omega}_{\perp}$ and parallel $\vec{\omega}_{||}$ velocity components in the drift frame. For the simple case of a constant particle kinetic energy [i.e., $W = m(\omega_{||}^2 + \omega_{\perp}^2)/2$], $\omega_{\perp}$ changes along $\vec{B}$ with the gradient of the magnetic field magnitude along $\vec{B}$ such that the magnetic moment $\mu = m\omega_{\perp}^2 / 2B$ of the particle is constant.

Adopting the guiding center theoretical construct for the motion of ions in the Io plasma torus and a planetary magnetic field description of a Jupiter-centered, tilted, and spinning dipole

magnetic field, Cummings et al. (1980) noted that $\bar{E}$ has the solution given by Eq. 4 and then assumed that the total drift velocity of an ion in the inertial frame is strictly corotational

$$\bar{\omega}_D = \bar{\Omega} \times \bar{r} \tag{7}$$

where $\bar{\Omega}$ is the System III angular rotation vector for Jupiter. Hence, in the non-inertial rotating frame (i.e., the so-called plasma rest frame), the electric field is zero, the drift velocity is zero, and the centrifugal force (that arises from the transformation to the non-inertial frame) and the magnetic gradient force along $\bar{B}$ are the only two remaining forces acting on the particle. The paper then addressed the questions as to what are the equilibrium position and bounce period of a particle along the magnetic field as a function of its kinetic energy W.

The basic solution outlined above will need to be generalized to include an east-west (dawn-dusk) electric field $\bar{E}_{e-w}$ in the plasma torus. This can be accomplished in a linear superposition by adding to the above solution an east-west field, $\bar{E}_{e-w}$, of the form

$$\bar{E}_{e-w} = \bar{E}_0 - (\bar{E}_0 \cdot \hat{b})\hat{b} , \tag{8}$$

where the electric field $\bar{E}_0$ has a suitable functional form so as to describe the behavior of the dawn-to-dusk directed electric field and $\hat{b}$ is a unit vector along $\bar{B}$. The solution for $\bar{E}_{e-w}$ is obviously constructed so as to satisfy the condition given by Eq. 4. The approximate solution for $\bar{B}$ of a tilted (or off-set tilted) spinning dipole should still be appropriate if the new polarization charge along the $\bar{B}$ field caused by $\bar{E}_{e-w}$ does not produce a significant current or a significant $\bar{B}$ field to alter the assumed dipole magnetic field solution. The generalized solution obtained by the linear superposition of the east-west electric field $\bar{E}_{e-w}$ will, however, produce a convective motion of the charged particles in the non-inertia rotating frame. A new plasmacentric reference frame $\tilde{L}$, as introduced by Smyth and Combi (1988a,b) and utilized by Smyth and Marconi (1998), will then need to be introduced to eliminate this convective motion of charged particles in the non-inertia rotating frame and hence provide a new so-called "rest frame" for the charged particles.

2.4 Convective Velocity for Plasma Subcorotation in the Plasma Torus

The best spatial information for the nature of the deviation from corotation of the plasma torus is that obtained by Brown (1994a,b) for simultaneous ground-based spectral measurements of the eastern (dawn) and western (dusk) ansa in the S^+ (6716, 6731 Å) emission lines. Figure 9 shows the average dawn and dusk profiles for the plasma deviation from corotation derived by Brown (1994b) from the sum of 222 spectra acquired over 53 nights of observations from December 2, 1991 to June 1, 1992. Inside of Io's orbit (vertical dashed line), the dawn and dusk profiles are essentially identical. The portion of the profiles inside of the S^+ brightness peaks,

which are located just inside of ~6 R_J, are, however, not an appropriate description of the inner deviation from corotation since the plasma emissions dim very rapidly for these smaller distances and this deviation from corotation signature is produced primarily by the plasma emissions that are located at foreground and background distances along the line of sight measurements. At the western (dusk) ansa, the plasma corotation deviation has a trough depth of ~3.2 km s^{-1} centered ~0.25 R_J outside of Io's orbit (dashed line) and has a half-width of perhaps

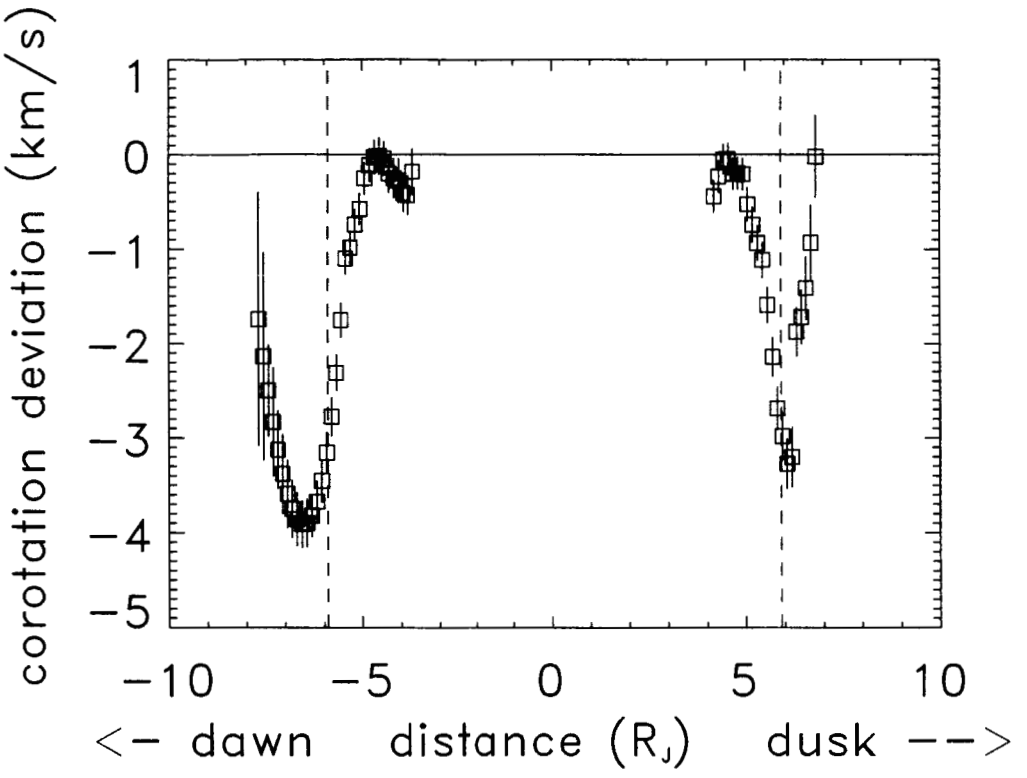

Figure 9. Corotational Deviation in the Io Plasma Torus. The average radial profiles for corotational deviation of the plasma torus at the eastern (dawn) and western (dusk) ansa as deduced from ground-based observations of S^+ (6716, 6731 Å) emission by Brown (1994b) are shown.

~0.5 R_J half way up the profile. The profile exhibits an east-west asymmetry, since the plasma corotation deviation at the eastern (dawn) ansa has a larger trough depth (~4 km s^{-1}) centered at ~0.55 R_J outside of Io's orbit (i.e., ~0.3 R_J radially outward from the dawn trough) and has a factor of two wider half-width (~1 R_J) half way up the profile. This same east-west asymmetry is also seen in S^+ (6716, 6731 Å) emission observations for a much smaller data set acquired in July 1994 before, during, and after the impact of comet Shoemaker-Levy 9 with Jupiter (Brown et al. 1995). Three key questions that arise from Figure 9 are: (1) why should subcorotation of the plasma torus exist all around Jupiter if it is driven by mass loading of new pickup ions that occurs primary near Io; (2) what part of the observed plasma corotation deviation pattern is

actually produced by mass loading from Io; and (3) why do the profiles for the plasma corotation deviation at the eastern (dawn) and western (dusk) ansa differ so significantly in their width, trough depth, and radial location?

An explanation for why subcorotation in the plasma torus should exist all around Jupiter for a current system that is driven by mass loading of new pickup ions occurring primary near Io (Inner Region source) has been given by Pontius (1995). In this picture, the transfer of angular momentum from Jupiter is driven by the mass loading of new pickup ions in the plasma torus, where the current system that connects directly to Jupiter's ionosphere is assumed to be confined predominately to plasma torus flux tubes located at or very near Io. The basic corotational lag then arises primarily in Jupiter's ionosphere (not in the plasma torus) by the subcorotational motion of neutrals slowed by plasma-neutral drag created by the closing in Jupiter's ionosphere of the Birkeland (field-aligned) current from Io. The dominant subcorotational electric field established in Jupiter's ionosphere is then mapped down along magnetic field lines into the plasma torus and there produces a corotational-lag velocity trough all around Jupiter. This subcorotational velocity trough is expected to be established over a time scale of a month or so because of the large moment of inertia of the neutrals in Jupiter's atmosphere and the slow response time for altering this neutral angular momentum by the plasma torus ions, which has a much smaller moment of inertia. The trough of the subcorotational velocity profile is therefore expected to be located on (or very near) Io's orbital path in Figure 1 (solid line) and hence azimuthally symmetric about Jupiter. The trough will therefore be positioned asymmetrically relative to the maximum plasma torus density, which is located on the dotted blue line inside of Io's orbit in Figure 1, and thereby will introduce a stronger corotational lag interaction with the ribbon near the eastern (dawn) ansa. The observed azimuthally asymmetric pattern of the plasma deviation from corotation at the dawn ansa in Figure 9 would then be attributed primarily to the dusk-to-dawn convective motion of the plasma produced by the east-west electric field that causes (1) a dusk-to-dawn shift in the plasma radial position of ~0.3 R_J and (2) a lower plasma velocity at a given distance from Jupiter in the dawn ansa profile due to the dusk-to-dawn shift in position and essentially a nearly constant rotational speed of the plasma along the shifted plasma trajectory. The lack of a supercorotation signature in Figure 9 inside of Io's orbit on the dusk side may indicate that the supercorotational speed introduced by the east-west electric field has been effectively canceled by the subcorotational speed introduced by mass loading from Io. The shape of the corotational lag profile in Figure 9 might also be possibly altered by differences in the conductivity of Jupiter's ionosphere in the pre-dawn night atmosphere as compared to the pre-dusk day atmosphere.

A different explanation for why a sub-corotation pattern may exist in the plasma torus around Jupiter has been given by Delamere et al. (2003). In this picture, the transfer of angular momentum from Jupiter is again driven by the mass loading of new pickup ions in the plasma torus, but the current system in the plasma torus is not assumed to be confined to flux tubes that

are predominately located very near Io where the instantaneous mass loading rate by the new pickup ions is thought to occur. In this picture, the angular momentum for the new pickup ions is initially largely supplied on a very short time scale by the loss of angular momentum from neighborhood plasma located in the much larger surrounding flux-tube volume. The loss of angular momentum from the neighborhood flux-tube volume is then re-supplied by the planet at a slower rate because the angular momentum transfer rate is limited by the closure current system that is now considered to be partially decoupled from Jupiter's ionosphere. The partial decoupling may be caused by the finite conductivity of Jupiter's ionosphere (Hill and Vasyliunas 2002) or by parallel electric fields (Delamere et al. 2003). The re-supplying of the angular momentum to the neighborhood plasma will therefore occur over a longer time scale, which is estimated to be of order a Jupiter rotation, and hence will occur over a spatially extended volume well downstream of Io and hence located around Jupiter. The location of the subcorotational velocity trough about Jupiter will therefore depend upon the circumplanetary variation of the source rate of new pickup ions at Io and will also be subject to the radial convective motions of the east-west electric field. From calculations of the S^+ source rate by Smyth and Marconi (1998; see their Figure 4), the production rate of new plasma from an Io point source (Inner Region source) is much larger (and indeed has its maximum value) when Io is near western (dusk) elongation (where the satellite is in the warm outer torus) rather than when Io is near eastern (dawn) elongation (where the satellite is in the cold inner torus). For this local-time variation of the source rate, the sub-corotational velocity trough would then be established primarily at or near Io's orbit at the western (dusk) ansa and would be shifted farther radially outside by ~0.3 R_J at the eastern (dusk) ansa, as indeed is observed to be the case in Figure 9. The subcorotational velocity trough would then be located on the red dashed-line circle in Figure 1 outside of Io's orbit and would be symmetrically positioned about the maximum density of the plasma torus that is located on the blue dotted-line circle inside of Io's orbit. For this configuration, the subcorotational velocity trough will provide on a circumplanetary scale a symmetric velocity shear impoundment (Pontius et al. 1998) of the maximum density of the plasma torus located on the blue dotted-line circle and hence would foster the development and stability of this maximum density (i.e., ribbon) structure.

In addition to an extended circumplanetary region in the plasma torus for the active transfer of angular momentum from Jupiter caused by the partial decoupling of the closure current system noted above for the Inner Region source, a larger spatial region about Io's orbit of subcorotation may also be caused by new pickup ions that are created by electron impact ionization and charge exchange of the spatially distributed neutrals for the Outer Region source. The circumplanetary distribution of the instantaneous net-mass loading rate of new pickup ions from O and S atoms in Io's corona and extended neutral clouds is shown in Figure 10 as calculated by Smyth and Marconi (2003a) for the satellite at western elongation and a System III longitude of 230°. In Figure 10a, the two-dimensional distribution of the instantaneous net mass loading rate, obtained by integrating the three-dimensional distribution along the magnetic field,

is very highly peaked about Io and hence asymmetrically distributed about Jupiter, has substantially forward and trailing arm enhancements about Io that are centered on its orbit, and has substantial enhancements in Io's vicinity that are asymmetrically distributed well outside of its orbit and behind (i.e., upstream of) the satellite. In Figure 10b, this asymmetric distribution about Io is clearly depicted by the one-dimensional System III longitude profile of the instantaneous net-mass loading rate obtained by integrating the two-dimensional distribution in

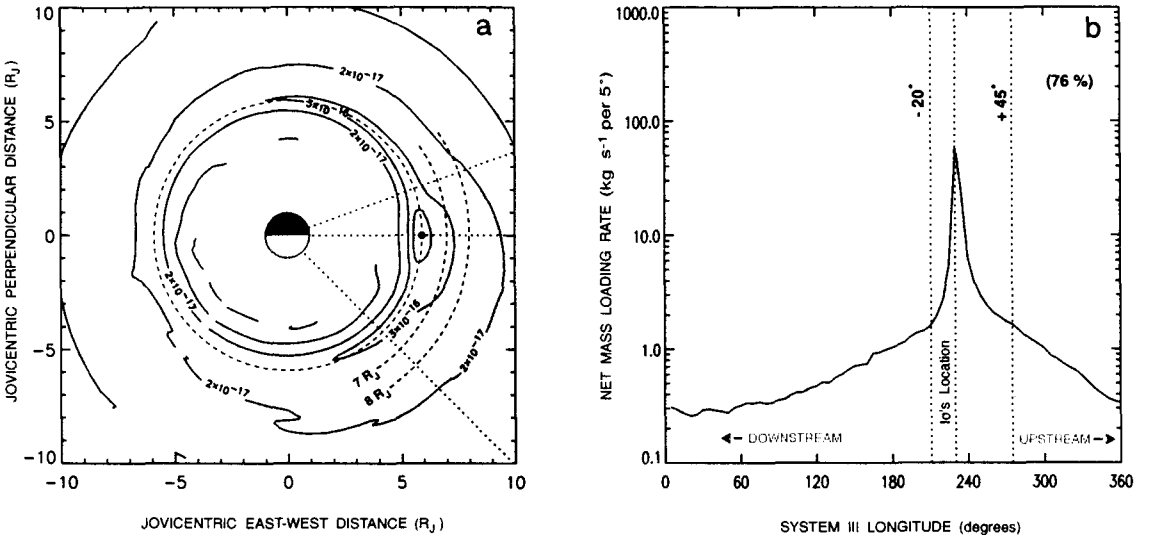

Figure 10. Net-Mass Loading Rate. The model calculated circumplanetary distribution for the instantaneous net-mass loading rate of the plasma torus determined by Smyth and Marconi (2003a) from the O and S pickup ion rates is shown in (a) in two dimensions (kg m^{-2} s^{-1}), having been integrated along the magnetic field, and in (b) in one dimension (kg s^{-1} per 5°) as a function of System III longitude, having been integrated, in addition, along the radial coordinate. The locations of Jupiter (half lit disk), Io's orbit (dashed circle), and Io (filled circle, on the dashed circle) at western elongation are indicated. The shaded region in (a) is bounded by two outer dashed lines located 20° and 45° on either side of the dashed line connecting Jupiter and Io. The locations of these same three dashed lines are also shown in (b) by the three vertical dashed lines and mark the boundaries between which 76% of the spatially-integrated net-mass loading rate of 154 kg s^{-1} is contained. In (a), the unmarked inner and outer contours are 3×10^{-15} kg m^{-2} s^{-1} and 2×10^{-18} kg m^{-2} s^{-1}, respectively.

Figure 10a over the radius coordinate. Within the shaded area for this asymmetric distribution in Figures 10a and 10b, bounded in System III longitude by lines at –20° downstream and +45° upstream of Io, most (117 kg s^{-1} or 76%) of the totally spatial-integrated instantaneous net-mass loading rate of 154 kg s^{-1} is concentrated. The spatial pattern for the total-mass loading rate (i.e., electron impact plus charge exchange processes) is similar. This net-mass loading rate for the Outer Region source is similar in magnitude but is more spatially distributed than the Inner Region source that is spatially concentrated at Io and hence may therefore influence the exact radial location at the western (dusk) ansa of the corotational lag trough relative to Io.

There then appears to be two different but likely paths in System III longitude and L shell about which the corotational lag velocity profile may be organized. First, if the current closure system is strongly coupled to Jupiter so that the angular momentum transfer to the instantaneous plasma loading rate is tightly spatially confined to near the initial creation positions of the new pickup ions very near Io and its immediate orbit vicinity, the corotational lag profile is expected to be created primarily in Jupiter's atmosphere and hence be organized in the plasma torus about Io's orbit, which is illustrated in Figure 1 by the solid black circle. Second, if the current closure system is partially decoupled from Jupiter so that the angular momentum transfer region to the instantaneous plasma loading rate is slowed and hence is spatially distributed well downstream of Io, the corotational lag profile is expected to be organized in the plasma torus about a dusk-to-dawn shifted trajectory such as the red dashed-line circle in Figure 1. It is furthermore likely that the mass loading rate may have corotational lag velocity profile components that are organized about both of these paths simultaneously. More effort will be directed in the second project year to refine our understanding of the path in System III longitude and L shell about which the corotational lag velocity profile is organized.

References

Bagenal, F. (1994) Empirical Model of the Io Plasma Torus: Voyager Measurements, *J. Geophys. Res.* **99**, 11043-11062.

Brown, M. E. (1994a) The Structure and Variability of the Io Plasma Torus, Ph.D. Thesis, Dept. of Astronomy, Univ. of California at Berkeley.

Brown, M. E. (1994b) Observations of Mass Loading in the Io Plasma Torus, *Geophys. Res. Letts.* **21**, 847-850.

Brown, M. E., E.J. Moyer, A.H. Bouchez, and H. Spinrad (1995) Comet Shoemaker-Levy 9: No Effect on the Plasma Torus, *Geophys. Res. Letts.* **22**, 1833-1835.

Cummings, W.D., A.J. Dessler and T.W. Hill (1980) Latitudinal Oscillation of Plasma within the Io Torus, *J. Geophys. Res.* **85**, 2108-2114.

Delamere, P.A., F. Bagenal, R. Ergun, and Y-J. Su (2003) Momentum Transfer between the Io Plasma Wake and Jupiter's Ionosphere, *J. Geophys. Res.* **108**(A6), 1241.

Hill, T.W. and V.M. Vasyliunas, (2002) Jovian Auroral Signature of Io's Corotational Wake, *J. Geophys. Res.* **107**(A12), pp. SMP27-1, Citel 1464, DOI 10.1029/2002JA009514.

Hones, E.H and J.E. Bergeson (1965) Electric Field Generated by a Rotating Magnetized Sphere, *J. Geophys. Res.* **70**, 4951-4958.

Oliversen, R.J., F. Scherb, W.H. Smyth, M.E. Freed, R.C. Woodward, M.L. Marconi, K.D. Retherford, O.L. Lupie, and J.P. Morgenthaler (2001) Sunlit Io Atmospheric [O I] 6300 Å Emission and the Plasma Torus, *J. Geophys. Res.* **106**, 26,183-26,193.

Paterson, W.R. (2000) private communication.

Pontius, D.H. (1995) Implications of Variable Mass Loading in the Io Torus: The Jovian Flywheel, *J. Geophys. Res.* **100**, 19,531-19,539.

Pontius, D.H., R.A. Wolf, T.H. Hill, R.W. Spiro, Y.S. Yang, and W.H. Smyth (1998) Velocity Shear Impoundment of the Io Plasma Torus, *J. Geophys. Res.* **103**, 19,935-19,946.

Smyth, W.H. and M.R. Combi (1988a) A General Model for Io's Neutral Gas Cloud. II. Application to the Sodium Cloud, *Ap. J.* **328**, 888-918.

Smyth, W.H. and M.R. Combi (1988b) A General Model for Io's Neutral Gas Cloud. I. Mathematical Description, *Ap. J. Supp.* **66**, 397-411.

Smyth, W.H. and M.L. Marconi (1998) An Explanation for the East-West Asymmetry of the Plasma Torus, *J. Geophys. Res.* **103**, 9091-9100.

Smyth, W.H. and M.L. Marconi (2003a) Nature of the Iogenic Plasma Source in Jupiter's Magnetosphere I. Circumplanetary Distribution, *Icarus* **166**, 85-106.

Smyth, W.H. and M.L. Marconi (2003b) Nature of the Iogenic Plasma Source in Jupiter's Magnetosphere II. Near-Io Distribution, *Icarus*, submitted.

Spitzer, L. (1952) Equations of Motion for an Ideal Plasma. *Ap. J.* **116**, 229-316.

Zhan, J. and T.W. Hill (2000) Drift Resonance and Stability of the Plasma Torus, *J. Geophys. Res.* **105**, 5555-5562.

REPORT DOCUMENTATION PAGE

Form Approved
OMB No. 0704-0188

Public reporting burden for this collection of information is estimated to average 1 hour per response, including the time for reviewing instructions, searching existing data sources, gathering and maintaining the data needed, and completing and reviewing the collection of information. Send comments regarding this burden estimate or any other aspect of this collection of information, including suggestions for reducing this burden, to Washington Headquarters Services, Directorate for Information Operations and Reports, 1215 Jefferson Davis Highway, Suite 1204, Arlington, VA 22202-4302, and to the Office of Management and Budget, Paperwork Reduction Project (0704-0188), Washington, DC 20503.

1. AGENCY USE ONLY *(Leave blank)*	2. REPORT DATE	3. REPORT TYPE AND DATES COVERED
	December 29, 2003	Annual, December 19 , 2002 to December 18, 2003

4. TITLE
Two-Dimensional Transport Studies for the Composition and Structure of the Io Plasma Torus

5. FUNDING NUMBERS
NASW-02003

6. AUTHORS
William H. Smyth

7. PERFORMING ORGANIZATION NAME(S) AND ADDRESS(ES)
Atmospheric and Environmental Research, Inc.
131 Hartwell Avenue
Lexington, MA 02421

8. PERFORMING ORGANIZATION REPORT NUMBER
P-1037

9. SPONSORING/MONITORING AGENCY NAME(S) AND ADDRESS(ES)
NASA Headquarters
Headquarters Contract Division
Washington, DC 20546

10. SPONSORING/MONITORING AGENCY REPORT NUMBER
NASW-02036

11. SUPPLEMENTARY NOTES

12a. DISTRIBUTION/AVAILABILITY STATEMENT

12b. DISTRIBUTION CODE

13. ABSTRACT *(Maximum 200 words)*

Research efforts in the first project year have been focused upon two basic quantities required to solve the two-dimensional plasma transport equations: (1) the assessment of the neutral-plasma reaction rates and the initiation of the calculations of their associated instantaneous ion production and loss rates, and (2) the investigation of the nature of the corotational lag velocity profiles for the plasma torus caused by mass loading from Io. Progress in both areas is reported.

14. SUBJECT TERMS	15. NUMBER OF PAGES
Io plasma torus, plasma structure and transport	23
	16. PRICE CODE

17. SECURITY CLASSIFICATION OF REPORT	18. SECURITY CLASSIFICATION OF THIS PAGE	19. SECURITY CLASSIFICATION OF ABSTRACT	20. LIMITATION OF ABSTRACT
Unclassified	Unclassified	Unclassified	Unlimited

NSN 7540-01-280-5500 Computer Generated STANDARD FORM 298 (Rev 2-89)
Prescribed by ANSI Std 239-18
298-102